Journal of Medical Imaging

MedicalImaging.SPIEDigitalLibrary.org

Use of a channelized Hotelling observer to assess CT image quality and optimize dose reduction for iteratively reconstructed images

Christopher P. Favazza
Andrea Ferrero
Lifeng Yu
Shuai Leng
Kyle L. McMillan
Cynthia H. McCollough

SPIE.

Christopher P. Favazza, Andrea Ferrero, Lifeng Yu, Shuai Leng, Kyle L. McMillan, Cynthia H. McCollough, "Use of a channelized Hotelling observer to assess CT image quality and optimize dose reduction for iteratively reconstructed images," *J. Med. Imag.* **4**(3), 031213 (2017), doi: 10.1117/1.JMI.4.3.031213.

Use of a channelized Hotelling observer to assess CT image quality and optimize dose reduction for iteratively reconstructed images

Christopher P. Favazza,* Andrea Ferrero, Lifeng Yu, Shuai Leng, Kyle L. McMillan, and Cynthia H. McCollough
Mayo Clinic, Department of Radiology, Rochester, Minnesota, United States

Abstract. The use of iterative reconstruction (IR) algorithms in CT generally decreases image noise and enables dose reduction. However, the amount of dose reduction possible using IR without sacrificing diagnostic performance is difficult to assess with conventional image quality metrics. Through this investigation, achievable dose reduction using a commercially available IR algorithm without loss of low contrast spatial resolution was determined with a channelized Hotelling observer (CHO) model and used to optimize a clinical abdomen/pelvis exam protocol. A phantom containing 21 low contrast disks—three different contrast levels and seven different diameters—was imaged at different dose levels. Images were created with filtered backprojection (FBP) and IR. The CHO was tasked with detecting the low contrast disks. CHO performance indicated dose could be reduced by 22% to 25% without compromising low contrast detectability (as compared to full-dose FBP images) whereas 50% or more dose reduction significantly reduced detection performance. Importantly, default settings for the scanner and protocol investigated reduced dose by upward of 75%. Subsequently, CHO-based protocol changes to the default protocol yielded images of higher quality and doses more consistent with values from a larger, dose-optimized scanner fleet. CHO assessment provided objective data to successfully optimize a clinical CT acquisition protocol. [DOI: 10.1117/1.JMI.4.3.031213]

Keywords: channelized Hotelling observer; computed tomography; radiation dose; iterative reconstruction; low contrast resolution.
Paper 17084SSRR received Mar. 30, 2017; accepted for publication Sep. 18, 2017; published online Oct. 3, 2017.

1 Introduction

The primary aims of iterative reconstruction (IR) are to reduce image noise and maintain or improve spatial resolution.[1] Indeed, IR techniques have been shown to successfully decrease the noise of CT images obtained at lower radiation dose levels.[1–3] Consequently, IR algorithms have been leveraged as tools to reduce patient dose, i.e., achieve similar image noise as a filtered backprojected (FBP) image at a fraction of the dose. For example, after the introduction of adaptive iterative dose reduction three-dimensional (AIDR 3D) image reconstruction software on the Toshiba CT scanner platform, the dose for default routine abdomen/pelvis protocols is substantially and automatically reduced—by upward of 70% to 75% relative to the full-dose FBP image.[4] However, whether low contrast spatial resolution can be maintained at these aggressive dose reduction levels has not been shown for this IR technique. This is critically important for many diagnostic tasks performed using a routine abdomen/pelvic CT exam, such as the detection and classification of low contrast liver lesions.

In fact, degradation of low contrast spatial resolution already has been shown for IR images obtained with overly aggressive dose reduction.[5–7] McCollough et al. have shown a loss of low contrast object detectability in IR images acquired at dose reductions of 50% or more relative to full-dose FBP images, despite equivalent image noise values.[7] While Solomon et al. have shown that images formed by IR and acquired using 75% less dose can achieve the same contrast to noise ratio as full-dose FBP images, this amount of dose reduction yielded an ∼8% degradation in object detectability.[6] In these studies, conventional measures of image quality, i.e., contrast to noise ratio or image noise, would suggest similar image quality; however, human observer assessment yielded different results. Importantly, due to dose-reduced IR images having equivalent noise and high contrast spatial resolution as the FBP images, this loss in low contrast spatial resolution may go unnoticed by the unsuspecting viewer, i.e., the radiologist tasked with exam interpretation. Consequently, important low contrast features may be missed or misinterpreted from images obtained with an insufficient number of photons, even when IR is used.

To address the aforementioned limitations of conventional image quality measurements in evaluating IR images, task-based image metrics from observer models are being leveraged.[8–19] Here, we present our investigation on low contrast object detectability in images reconstructed with Toshiba's AIDR 3D IR algorithm using a channelized Hotelling observer (CHO) model. More specifically, we applied a CHO to determine the amount of dose reduction that is achievable with AIDR 3D while still maintaining equivalent low contrast object conspicuity as that of a full-dose FBP image. Ultimately, results from this investigation were used to optimize our routine abdomen/pelvis acquisition protocol for our fleet of Toshiba CT scanners.

2 Methods

2.1 *Image Acquisition*

An 18-cm-diameter cylindrical phantom containing 18 spherical objects and 6 cylindrical objects (Spiral/Helical CT Phantom,

*Address all correspondence to: Christopher P. Favazza, E-mail: favazza.christopher@mayo.edu

2329-4302/2017/$25.00 © 2017 SPIE

Model 061 CIRS, Norfolk, Virginia) was imaged with a 160-slice CT scanner (Aquilion Prime 160, Toshiba America Medical Systems, Tustin, California). All spherical and cylindrical objects were centered along the logical z-axis of the phantom. Three of the six cylinders were aligned with the phantom in parallel; the other three were aligned perpendicularly. Thus, the center cross section of the phantom contained 21 disk objects (18 spheres and 3 cylinders) and 3 rectangle objects (Fig. 1). The 21 disk objects possessed seven different diameters (2.4, 3.2, 4, 4.8, 6.3, 9.5, and 10 mm) and three different contrast levels relative to background (nominal CT numbers: −10, −15, and −25 HU, which were confirmed by measurement of the associated rectangular object).

The phantom was scanned at eight different tube current settings with a 0.5-s gantry rotation time and a pitch of 0.813 at 120 kV. Automatic exposure control (AEC) was not used. One-millimeter-thick images were reconstructed at 1-mm intervals using FBP and an IR algorithm (AIDR 3D, Toshiba America Medical Systems) at three strength settings: mild, standard, and strong. For each tube current setting, the phantom was scanned 100 times. A summary of the experimental parameters is shown in Table 1.

The selection of the eight tube current settings was as follows. First, settings were found that yielded image noise values equal to predefined target values for FBP reconstructed images for small, medium, and large size patients—12, 17.5, and 22 HU, respectively.[20] Specifically, 180, 90, and 60 mA were used to simulate "full-dose" images and noise levels for small, medium, and large patient sizes. Then, tube current settings were calculated for different amounts of dose reduction: ~25%, 50%, 66%, and 75%. Scanner software restricted available tube current settings and prevented exact 25% and 75% dose reduction for the three surrogate patient sizes. Notably, a 75% dose reduction was also not possible for the "large patient" tube current setting, which was below the minimum limit of the x-ray tube. Where possible, the same tube current values were used for different "patient size" data to reduce image acquisitions. Correspondingly, eight tube current settings were used to simulate different levels of dose reduction for small, medium, and large surrogate patient sizes (see Table 2).

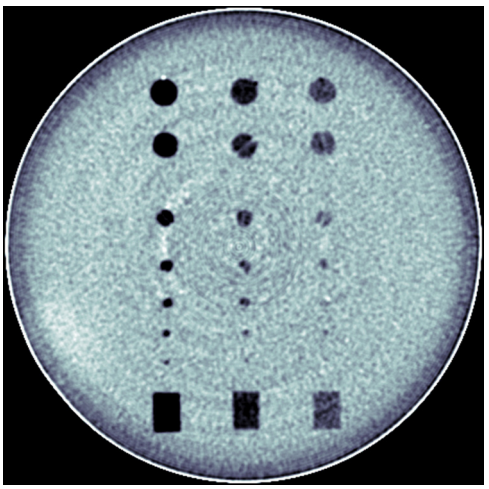

Fig. 1 An ensemble average image of the phantom's center showing the 21 disk objects evaluated with the CHO and the three rectangular objects used to confirm object contrast levels. The subtle rings are not visible in individual images due to masking by noise, and are apparent only in this ensemble average image.

Table 1 List of experimental and scan parameters.

Parameter	Value
Tube potential	120 kV
Rotation time	0.5 s
Pitch	0.813
Tube current	8 fixed settings (see Table 2)
Scan length	420 mm
Collimation	40 mm (0.5 mm × 80)
Convolution kernel	FC18
Reconstruction algorithms	(1) FBP; (2) AIDR 3D-mild; (3) AIDR 3-D-standard; (4) AIDR 3D-strong
Slice thickness/interval	1 mm/1 mm
Number scans/setting	100

Table 2 Relative dose and fixed tube current setting for the different simulated patient sizes. Because only one low contrast detectability phantom size was available, different tube current settings were used to achieve noise levels representing scans of different sizes of patients.

Dose	Small (FBP noise = 12 HU)	Medium (FBP noise = 17.5 HU)	Large (FBP noise = 22 HU)
Full dose	180 mA	90 mA	60 mA
75% dose[a]	140 mA	70 mA	45 mA
50% dose	90 mA	45 mA	30 mA
33% dose	60 mA	30 mA	20 mA
25% dose[b]	45 mA	20 mA	NA

[a]Indicates 77% dose for the small and medium size settings.
[b]Indicates 22% for the medium size setting.

2.2 *Observer Model*

A CHO was developed and tasked with determining object detectability. Images were channelized with Gabor filters consisting of five different spatial frequency passbands (center frequencies: $\frac{3}{256}$, $\frac{3}{128}$, $\frac{3}{64}$, $\frac{3}{32}$, and $\frac{3}{16}$ cycles/pixel), four rotation angles (0 deg, 45 deg, 90 deg, and 135 deg), and a single phase (0 deg), yielding 20 total channels. An internal noise factor identical to that used by Yu et al. was also incorporated into the model such that the CHO's performance matched human observer performance.[9] Notably, fewer channels were used in the model applied in this study as compared to the model used by Yu et al. Fewer channels were used in this model as it has been shown that using fewer channels improves statistical

performance of a CHO and requires fewer repeated scans, given that the channel selection is appropriate for the objects of interest.[21,22] Additionally, the 20-channel CHO model was validated against previously acquired human observer and observer model data presented by Yu et al.[9] More specifically, the 20-channel CHO described above was challenged with a two-alternative forced choice (2AFC) test using the same image data as used by Yu et al.[9] "percent correct" (Pc) values from the 2AFC tests for the different sized cylindrical objects (3, 6, and 9 mm diameter; and −15 HU contrast) were determined for different reconstruction algorithms and dose settings, as described by Yu et al.[9] The Pc differences between the 20-channel CHO performance and both human observers and the 60-channel CHO were computed.

2.3 *Image Analysis*

One hundred "signal-present" images were obtained from the center of the phantom, which contained the 21 disk objects. One hundred background images were obtained from a uniform region of the phantom near its edge. For the three largest diameter disks, 60×60 pixel regions of interests (ROIs) were centered on the objects. For the remaining objects, 40×40 pixel ROIs were centered on the objects. (Due to the closer spacing of smaller objects, it was necessary to use a smaller ROI such that only the object of interest was contained in the ROI. A previous study has shown that these differences in ROI size do not affect CHO performance.[23]) For all objects, ROIs were centered in the same $x - y$ positions in the background images to obtain "signal-absent" images. These sets of signal-present and signal-absent ROIs were used to train and test the model using the "resubstitution" method, by which the training and testing sets of images are identical.[24] The area under the receiver operator characteristic curve (AUC) was used as a figure of merit for the model's performance. AUC values were compared for the different acquisition and reconstruction conditions. Likewise, conventional image noise values were measured in all sets of images and subsequently compared.

2.4 *Clinical Application*

Based on the CHO results, routine abdomen/pelvis protocol acquisition parameters were changed on Toshiba scanners in our clinical practice to achieve comparable low contrast detectability as our main clinical site, which has previously been studied and optimized.[20,25,26] Exam dose data were collected over a period of 1 year prior to the protocol change and over a period of 6 months after the change. Average pre- and postintervention $CTDI_{vol}$ values were computed and compared with $CTDI_{vol}$ values from exams at our main clinical site, which does not use Toshiba CT scanners.

3 Results

3.1 *Observer Model Validation*

A comparison of Pc values from 2AFC tests show that the 20-channel CHO model implemented in this study agreed well with both human observers and the 60-channel CHO used by Yu et al.[9]—an average of 2.1% and 2% difference in Pc values, respectively (Table 3).

Table 3 Absolute differences in Pc between the 20-channel CHO and both human and model observers data from Yu et al.[9]

			Absolute difference of percent correct with 20-channel CHO	
Reconstruction	mAs	Object size	Human observer (%)	CHO (Yu)[9] (%)
FBP (B40)	60	Small	4.1	3.9
		Medium	2.7	6.1
		Large	1.9	2.9
	120	Small	0.2	2.7
		Medium	2.1	3.6
		Large	1.0	0.2
	240	Small	4.0	1.9
		Medium	2.6	1.0
		Large	0.0	0.0
	360	Small	1.8	0.2
		Medium	0.0	0.0
		Large	0.2	0.0
	480	Small	0.5	1.0
		Medium	0.0	0.0
		Large	0.5	0.0
IR (I40-3)	60	Small	5.6	4.0
		Medium	4.0	5.7
		Large	2.9	4.3
	120	Small	9.1	2.0
		Medium	0.5	2.0
		Large	0.6	0.2
Average			2.1	2.0

3.2 *Observer Model Comparison*

A qualitative visual inspection of the images demonstrated that object conspicuity decreases with decreasing dose for each reconstruction algorithm. As an example, sample phantom images of the 4.8-mm-diameter object at −25 HU contrast relative to background clearly show a reduction in object conspicuity for the small patient reconstruction settings as dose is reduced (Fig. 2). For quantitative assessment, there are many objects that can be interrogated with the CHO model; however, the detectability of many objects was either well above or well below the human detection threshold. By considering only the objects that did not yield saturated AUC values (i.e., obvious objects) or values at the cusp of reliable human detection, relevant detectability statistics were derived across a spectrum of

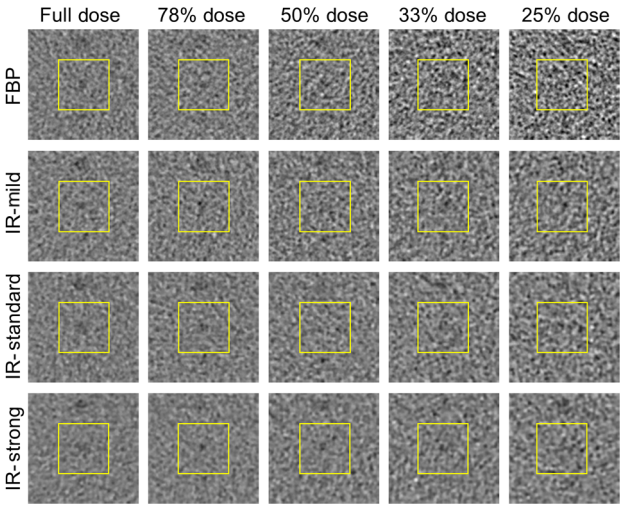

Fig. 2 Sample object-present images for the surrogate small patient size at each dose setting and reconstruction method.

Table 4 Objects used to determine the average, normalized AUC values.

Diameter (mm)	Contrast level (HU)
4.0	−25
4.8	−25
6.3	−15
9.5	−15
10	−10

object size and contrast. Specifically, five objects yielded $0.65 < \mathrm{AUC} < 1$ for FBP images across all dose levels and are listed in Table 4 and shown in Fig. 3(a). AUC values from these objects were used to generate the average score for each combination of reconstruction algorithm, size setting, and dose level, as determined by

$$\overline{\widehat{\mathrm{AUC}}}(r,s,d) = \frac{1}{n}\sum_{\mathrm{in}} \frac{\mathrm{AUC}(r,s,d)}{\mathrm{AUC}(r_0,\ s,d_0)},$$

where $\mathrm{AUC}(r,s,d)$ is the AUC value for a given: reconstruction algorithm, r; size setting, s; and dose level d; n is the object number, and r_0 and d_0 represent the FBP reconstruction algorithm and the full-dose level, respectively.

These $\overline{\widehat{\mathrm{AUC}}}(r,s,d)$ results agree the visual inspection of the images in which the relative $\overline{\widehat{\mathrm{AUC}}}$ values decrease with decreasing dose (Fig. 3). Importantly, a comparison of the full-dose FBP $\overline{\widehat{\mathrm{AUC}}}$ values with those obtained from images acquired with 22% to 25% dose reduction and reconstructed with AIDR 3D (standard strength) indicates that these sets of $\overline{\widehat{\mathrm{AUC}}}$ are statistically similar (Table 5). A comparison of the full-dose FBP $\overline{\widehat{\mathrm{AUC}}}$ values with those obtained from images acquired with 50% or greater dose reduction and reconstructed with AIDR 3D (standard strength) showed significant differences between the sets of $\overline{\widehat{\mathrm{AUC}}}$ values (Table 5). When the dose was reduced by 75% of the full-dose FBP value—similar to the default and automatic reduction possible with this scanner platform, $\overline{\widehat{\mathrm{AUC}}}$ values dropped by an average of 12.4%.

Although the CHO performance was significantly poorer for images acquired with 50% or lower dose (Table 5), the image noise was similar (within one standard deviation) or lower for dose-reduced images reconstructed with AIDR 3D (Fig. 4). More specifically, image noise values from full-dose FBP images were similar (within 2 HU) or greater than images

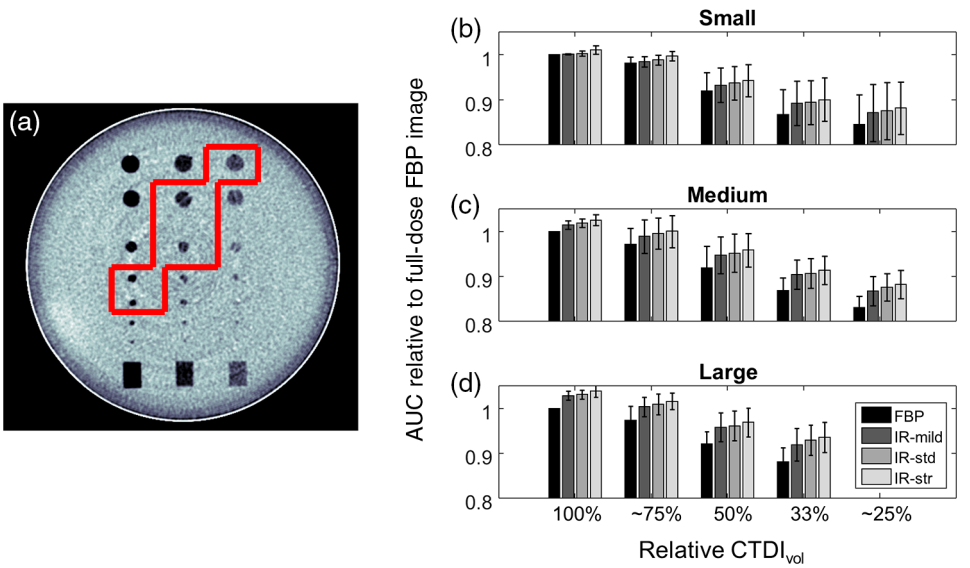

Fig. 3 (a) Center image of phantom with evaluated objects outlined in red. (b–d) Normalized AUC values (relative to full-dose FBP image) for (b) small, (c), medium, and (d) large patient size as a function of $\mathrm{CTDI_{vol}}$ relative to full-dose acquisition. Error bars represent the standard deviation of AUC values. †Indicates 77% $\mathrm{CTDI_{vol}}$ for the small and medium size settings. *Indicates 22% $\mathrm{CTDI_{vol}}$ for the medium size setting.

Table 5 Difference in average, normalized AUC values for the full-dose FBP images and AIDR 3D (standard strength) images acquired at different dose levels for each size setting. Associated *p*-values from two-tailed student *t*-test are listed from each difference value.

Dose relative to full-dose FBP	Small		Medium		Large	
	$\Delta\widehat{AUC}$	*P*-value	$\Delta\widehat{AUC}$	*P*-value	$\Delta\widehat{AUC}$	*P*-value
100%	+0.002	0.4	+0.019	0.002	+0.031	0.0001
75%[a]	−0.012	0.05	−0.004	0.8	+0.009	0.4
50%	−0.063	0.005	−0.048	0.03	−0.039	0.03
33%	−0.106	0.001	−0.094	0.0002	−0.071	0.0015
25%[b]	−0.124	0.002	−0.124	0.00	—	—

[a]Indicates 77% dose for the small and medium size settings.
[b]Indicates 22% dose for the medium size setting.

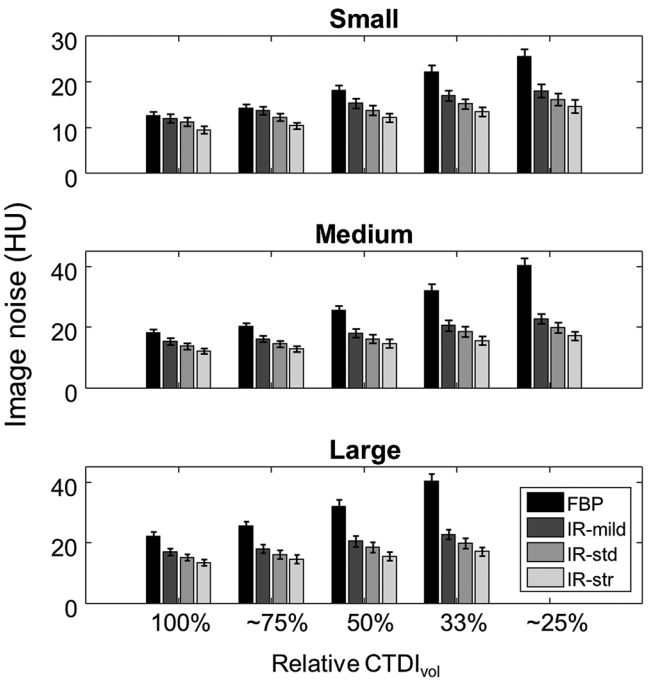

Fig. 4 Plots of image noise as function of $CTDI_{vol}$ relative to the full-dose acquisition setting for (a) small, (b) medium, and (c) large patient size classes. Error bars represent the standard deviation of image noise values. †Indicates 77% $CTDI_{vol}$ for the small and medium size settings. *Indicates 22% $CTDI_{vol}$ for the medium size setting.

reconstructed with AIDR 3D (standard strength) for dose reductions of 50%, 25%, and 33% for small, medium, and large size classes, respectively.

3.3 *Clinical Implementation*

Substantial differences in dose were found from a comparison of $CTDI_{vol}$ values from routine abdomen/pelvis exams at our main clinical site (non-Toshiba scanners) with those from our Toshiba scanners, which used the default amount of dose reduction associated with AIDR 3D (upward of 70% to 75%). Over a 1-year period prior to CHO-based protocol changes to our Toshiba scanners, the average $CTDI_{vol}$ value from our main site was almost twice that from our fleet of Toshiba scanners: 14.8 mGy ($n = 10074$) versus 7.7 mGy ($n = 4205$), as shown in Fig. 5.

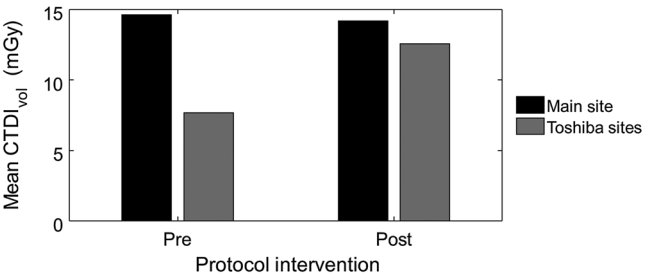

Fig. 5 Average $CTDI_{vol}$ values from routine abdomen/pelvis exams performed over a 1-year period prior to CHO-based protocol changes and over a 6-month period after the CHO-based protocol changes were implemented. Exam data were pulled from our main clinical site (non-Toshiba scanners) and our fleet of Toshiba scanners.

Following the results from the CHO-based evaluation of low contrast spatial resolution, the routine abdomen/pelvis acquisition protocol on our Toshiba scanners was adjusted. Namely, a size-specific image noise target (i.e., SD value) was instituted, and importantly, the SD value was set such that it yielded 25% dose reduction relative to the target image noise value for FBP reconstructed images. Special scanners settings were required to circumvent the default, automatic dose reduction associated with AIDR 3D.

The scanner's AEC system, SUREExposure, varies x-ray output based on the reconstruction method, which is determined by a specific SUREExposure setting, i.e., the selected SUREIQ preset group of parameters. A new SUREIQ preset was created to

Table 6 SUREIQ settings for the default protocol and modified protocol.

SUREIQ parameters	Default settings	Modified settings
Convolution kernel	FC18	FC18
Hybrid	OFF	OFF
Organ-specific reconstruction	Body	Body
Recon process	AIDR 3D standard	OFF
Image filter	OFF	OFF

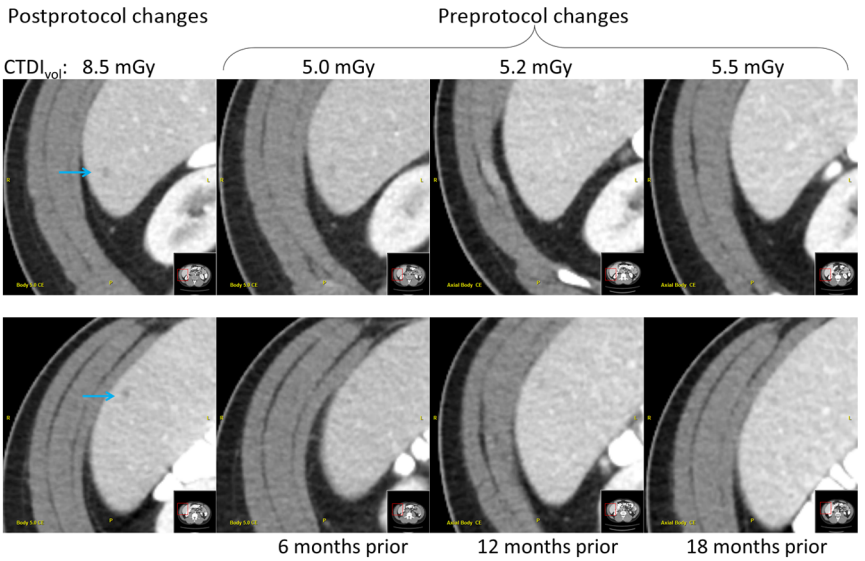

Fig. 6 Example images from four serial exams of a single patient obtained before and after the protocol intervention. Notably, two small potential cysts (denoted by the blue arrows) were identified for follow-up in the exam only after protocol changes were made to improve low contrast detectability.

indicate FBP reconstruction. The specific parameters are shown in Table 6. However, the image reconstruction settings were selected to cause the images to be formed with AIDR 3D. This configuration instructed $^{\text{SURE}}$Exposure to generate the requisite x-ray output to achieve an image noise value equal to the selected SD value for FBP reconstructed images and enabled the user to intuitively control dose reduction (i.e., dose relative to a full-dose FBP acquisition) through increasing the SD value.

After these changes to the protocol, data were collected over a 6-month period and compared. Results show that average CTDI_{vol} values were much similar: 14.2 mGy (main site; $n = 6157$) versus 12.6 mGy (Toshiba sites; $n = 1387$), as shown in Fig. 5. Further, qualitative assessment of exams before and after constraining dose reduction to 25% of the full-dose FBP value demonstrated material improvement in the low contrast detectability. As an example, Fig. 6 shows images from four serial exams of the same patient (three exams) before and (one exam) after the protocol changes. Notably, small potential cysts were noted in the radiologist's exam interpretation only after the protocol changes, despite being very subtly visible in the prior exams with knowledge of the respective locations.

4 Discussion

The results from this investigation support previous findings, which demonstrated that excessively reducing dose will lead to a reduction in low contrast object detectability in CT images, despite the use of iterative reconstruction techniques. Further, conventional image quality metrics such as image noise (i.e., standard deviation in CT number) may not fully characterize the diagnostic quality of iteratively reconstructed images—particularly for protocols that rely on low contrast spatial resolution. Rather, reduction of low contrast spatial resolution may not be fully appreciated by the radiologist with IR images, as the image noise values can be similar to FBP images that possessed greater low contrast spatial resolution. This imperceptible image quality reduction could lead to situations in which a radiologist is unable to identify images with insufficient diagnostic quality, thus leading to potentially dangerous scenarios in which the radiologist is unaware of what they do not see. In fact, the reduced dose levels in the practice may be celebrated, unaware that some clinically critical diagnostic tasks, such as the detection of liver metastases, may have been compromised.

A comparison of image noise across different dose settings indicated that AIDR 3D is applied more or less aggressively for images with higher or lower input noise, respectively. This observation is consistent with the vendor's description of their algorithm.[4] Thus, if using patient size-specific image noise targets, AIDR 3D will be applied more aggressively for image data from larger sized patients (i.e., higher input noise), whereas, it will be applied less aggressively for image data from smaller sized patients (i.e., lower input noise). Notably, CHO performance results demonstrated that the amount of input image noise, and hence the aggressiveness of AIDR 3D's application, did not influence the amount by which radiation dose could be reduced without loss of low contrast spatial resolution. A comparison of the ~75% dose images revealed that AIDR 3D reduced image noise by ~37% for the large patient size and only 14% for the small patient size, as compared to the respective FBP images at the same dose settings. However, CHO results indicated that a similar amount of dose reduction was possible with AIDR 3D (22% to 25%) without loss of low contrast object detectability for both the small and large patient size-specific noise image targets. Importantly, this result enables a straightforward and simple approach to leverage the dose reduction capabilities of AIDR 3D for size-specific protocols, achieving, for example, a 22% to 25% reduction for all size classes or FBP image noise targets.

A comparison of average CTDI_{vol} values from our routine abdomen/pelvis exams before and after protocol changes served to corroborate the CHO performance results. Prior to the change in acquisition settings, the roughly 50% dose difference between the Toshiba scanners and our main site scanner fleet could not be justified by differences in scanner hardware and software, or average patient size. Although the objective of the protocol changes was not to match dose with scanners and protocols from our main site, similar values were expected between both sets of scanners for equivalent diagnostic performance.

After the changes, the $CTDI_{vol}$ values were much closer between the sets of scanners and protocols, and the small difference could be explained by differences in patient cohort, average scanner age (and dose efficiency), and small image quality differences.

Although the CHO provides task-based image quality assessment, it is limited. In general, the application of a CHO provides assessment of a single task (e.g., detection of single object), just one criterion for an exam that has multifactor criteria for sufficient diagnostic image quality. However, the experimental design of this investigation enabled assessment of the detectability of multiple objects of different sizes and contrasts, and thereby represents multiple tasks. Because the range of tasks in this investigation covered a spectrum of the objects near the limit of human detection that are important for diagnosis in the abdomen and pelvis, they provided a relatively comprehensive assessment of diagnostic performance. In addition to low contrast detectability, there are other factors important to the diagnostic quality of an image but not assessed by the CHO. For example, the results from this investigation suggest that image quality (i.e., low contrast object conspicuity) monotonically increases with increasing AIDR 3D strength. AUC values consistently improve with AIDR 3D strength. The "strong" strength setting showed the highest AUC compared to other reconstruction settings for the same acquisition. However, use of a strong AIDR 3D setting could change the overall appearance and texture of the image too much, making it unacceptable to the radiologist. Consequently, other factors must still be considered when establishing or modifying acquisition protocols.

Another limitation of this study included the use of a single phantom size for determining the impact of AIDR 3D on size-specific protocols/noise targets. However, the primary objective of this investigation was to assess the behavior of AIDR 3D and resulting low contrast object detectability as a function of input image noise quantity, assuming image noise-based behavior is consistent over physically different patient sizes. Further, this assumption of applicability to different patient sizes was supported by the results from the clinical protocol modifications in which image quality improved and dose increased by a reasonable amount for a patient cohort containing a range of sizes.

5 Conclusions

This CHO-based investigation of low contrast detectability indicated that the dose reduction for a routine abdomen/pelvis protocol stemming from default acquisition settings associated with AIDR 3D (~70% to 75%) yielded images with significantly poorer low contrast object conspicuity. Further, this loss of low contrast detection performance could be obscured by relatively low image noise, which is a traditional marker to connote the overall quality of an image. Observer model assessment shows that the use of AIDR 3D can enable 22% to 25% dose reduction for a routine abdomen/pelvis exam without loss of low contrast object detectability, as compared to a full-dose FBP image, similar to findings in other studies. Lastly, implementing CHO-performance results through changes in acquisition parameters resulted in qualitatively improved images as well as patient dose levels that were more consistent with a large fleet of dose-optimized scanners and protocols.

Disclosures

Disclosure of potential conflict of interest: CHM receives grant funding from Siemens Healthcare, which is unrelated to this work.

Acknowledgments

Research reported in this article was supported by the National Institutes of Health under award numbers R01EB17095 and U01EB17185. The content is solely the responsibility of the authors and does not necessarily represent the official views of the National Institutes of Health.

References

1. A. Padole et al., "CT radiation dose and iterative reconstruction techniques," *Am. J. Roentgenol.* **204**(4), W384–W392 (2015).
2. S. Ono et al., "Improved image quality of helical computed tomography of the head in children by iterative reconstruction," *J. Neuroradiol.* **43**(1), 31–36 (2016).
3. K. A. Abdullah et al., "Radiation dose and diagnostic image quality associated with iterative reconstruction in coronary CT angiography: a systematic review," *J. Med. Imaging Radiat. Oncol.* **60**(4), 459–468 (2016).
4. E. Angel, "AIDR 3D iterative reconstruction: integrated, automated and adaptive dose reduction," Tustin, California (2012).
5. J. M. Kofler et al., "Assessment of low-contrast resolution for the American College of Radiology computed tomographic accreditation program: what is the impact of iterative reconstruction?" *J. Comput. Assist. Tomogr.* **39**(4), 619–623 (2015).
6. J. Solomon et al., "Effect of radiation dose reduction and reconstruction algorithm on image noise, contrast, resolution, and detectability of subtle hypoattenuating liver lesions at multidetector CT: filtered back projection versus a commercial model-based iterative reconstruction algorithm," *Radiology* **284**(3), 777–787 (2017).
7. C. H. McCollough et al., "Degradation of CT low-contrast spatial resolution due to the use of iterative reconstruction and reduced dose levels," *Radiology* **276**(2), 499–506 (2015).
8. J. G. Ott et al., "Assessment of low contrast detection in CT using model observers: developing a clinically-relevant tool for characterising adaptive statistical and model-based iterative reconstruction," *Z. Med. Phys.* **27**, 86–97 (2016).
9. L. Yu et al., "Prediction of human observer performance in a 2-alternative forced choice low-contrast detection task using channelized Hotelling observer: impact of radiation dose and reconstruction algorithms," *Med. Phys.* **40**(4), 041908 (2013).
10. J. Solomon and E. Samei, "Correlation between human detection accuracy and observer model-based image quality metrics in computed tomography," *J. Med. Imaging* **3**(3), 035506 (2016).
11. S. Leng et al., "Correlation between model observer and human observer performance in CT imaging when lesion location is uncertain," *Med. Phys.* **40**(8), 081908 (2013).
12. Y. Zhang et al., "Correlation between human and model observer performance for discrimination task in CT," *Phys. Med. Biol.* **59**(13), 3389–3404 (2014).
13. F. R. Verdun et al., "Image quality in CT: from physical measurements to model observers," *Phys. Med.* **31**(8), 823–843 (2015).
14. O. Christianson et al., "An improved index of image quality for task-based performance of CT iterative reconstruction across three commercial implementations," *Radiology* **275**, 132091 (2015).
15. A. Wunderlich and F. Noo, "Evaluation of the impact of tube current modulation on lesion detectability using model observers," in *30th Annual Int. Conf. of the IEEE Engineering in Medicine and Biology Society*, pp. 2705–2708, IEEE (2008).
16. A. Wunderlich and F. Noo, "Image covariance and lesion detectability in direct fan-beam x-ray computed tomography," *Phys. Med. Biol.* **53**(10), 2471–2493 (2008).
17. S. Richard et al., "Predictive models for observer performance in CT: applications in protocol optimization," *Proc. SPIE* **7961**, 79610H (2011).
18. B. Chen et al., "Evaluating iterative reconstruction performance in computed tomography," *Med. Phys.* **41**(12), 121913 (2014).
19. J. Solomon et al., "Comparison of low-contrast detectability between two CT reconstruction algorithms using voxel-based 3D printed textured phantoms," *Med. Phys.* **43**(12), 6497–6506 (2016).
20. C. P. Favazza et al., "A cross-platform survey of CT image quality and dose from routine abdomen protocols and a method to systematically standardize image quality," *Phys. Med. Biol.* **60**(21), 8381–8397 (2015).

21. L. Yu et al., "Correlation between a 2D channelized Hotelling observer and human observers in a low-contrast detection task with multislice reading in CT," *Med. Phys.* **44**, 3990–3999 (2017).
22. C. Ma et al., "Impact of number of repeated scans on model observer performance for a low-contrast detection task in computed tomography," *J. Med. Imaging* **3**(2), 023504 (2016).
23. A. Ferrero et al., "Practical implementation of channelized Hotelling observers: effect of ROI size," *Proc. SPIE* **10132**, 101320G (2017).
24. R. M. Gagne, B. D. Gallas, and K. J. Myers, "Toward objective and quantitative evaluation of imaging systems using images of phantoms," *Med. Phys.* **33**(1), 83–95 (2006).
25. J. G. Fletcher et al., "Pilot study of detection, radiologist confidence and image quality with sinogram-affirmed iterative reconstruction at half-routine dose level," *J. Comput. Assist. Tomogr.* **37**(2), 203–211 (2013).
26. J. G. Fletcher et al., "Observer performance in the detection and classification of malignant hepatic nodules and masses with CT image-space denoising and iterative reconstruction," *Radiology* **276**(2), 465–478 (2015).

Christopher P. Favazza, PhD, is an assistant professor of medical physics at the Mayo Clinic. He earned a PhD in physics from Washington University in St. Louis in 2008. His research interests include the development and clinical implementation of diagnostic and interventional radiology applications involving CT, MR, and optical imaging modalities.

Andrea Ferrero, PhD, graduated in physics engineering from the Polytechnic of Turin, Italy, followed by a master's degree in medical imaging at the Royal Institute of Technology in Stockholm, Sweden, and a PhD in biomedical engineering from the University of California, Davis. Currently, he is a clinical medical physics resident in the Department of Radiology at the Mayo Clinic, with a research focus on diagnostic and interventional CT imaging.

Lifeng Yu received his BS degree in nuclear physics in 1997 and an MEng degree in nuclear technology in 2000 both from Beijing University, and his PhD in medical physics from the University of Chicago in 2006. He is an associate professor of medical physics at the Mayo Clinic. His research interests include CT physics, image quality assessment, and spectral CT.

Shuai Leng, PhD, received his BS degree in engineering physics in 2001, an MS degree in engineering physics in 2003 from Tsinghua University, and his PhD in medical physics in 2008 from the University of Wisconsin, Madison. He is an associate professor of medical physics at the Mayo Clinic in Rochester, MN. He has authored over 100 peer-reviewed articles. His research interests are technical development and clinical application of x-ray and CT imaging.

Kyle L. McMillan: Biography is not available.

Cynthia H. McCollough, PhD, is a professor of radiological physics and biomedical engineering at the Mayo Clinic, where she directs the CT Clinical Innovation Center. Her research interests include CT dosimetry, advanced CT technology, and new clinical applications, such as dual-energy and multispectral CT. She is an NIH-funded investigator, and is active in numerous professional organizations. He is a fellow of the AAPM and ACR. She received her doctorate from the University of Wisconsin in 1991.